Low-energy model and electron-hole doping asymmetry of single-layer Ruddlesden-Popper iridates

Alexander Hampel, Christoph Piefke, and Frank Lechermann
I. Institut für Theoretische Physik, Universität Hamburg D-20355 Hamburg, Germany
(Received 16 April 2015; published 24 August 2015)

We study the correlated electronic structure of single-layer iridates based on structurally undistorted Ba_2IrO_4. Starting from the first-principles band structure, the interplay between local Coulomb interactions and spin-orbit coupling is investigated by means of rotational-invariant slave-boson mean-field theory. The evolution from a three-band description towards an anisotropic one-band ($J = 1/2$) picture is traced. Single-site and cluster self-energies shed light on competing Slater- and Mott-dominated correlation regimes. A nodal/antinodal Fermi-surface dichotomy is revealed at strong coupling, with an asymmetry between electron and hole doping. Electron-doped iridates show clearer tendencies of Fermi-arc formation, reminiscent of hole-doped cuprates.

DOI: 10.1103/PhysRevB.92.085141 PACS number(s): 71.27.+a, 71.18.+y, 71.30.+h, 71.70.Ej

I. INTRODUCTION

Iridum oxides based on the Ruddlesden-Popper series pose a particular challenging electronic structure problem [1–3]. The cooperation of strong spin-orbit coupling (SOC) with $5d$-shell Coulomb interactions stabilizes insulating phases at stoichiometry below room temperature. Since these compounds usually show also antiferromagnetic (AFM) ordering, it is debated if Mott or Slater mechanisms rule the observed insulating states [4–6]. Despite formally assumed weaker electronic correlations, the question arises if iridates still display deeper analogies to layered ruthenates or high-T_c cuprates in view of non-BCS superconducting properties [7].

While the Sr compound of single-layer ruthenates has ideal tetragonal symmetry, the sister compound Sr_2IrO_4 shows tilting of the IrO_6 octahedra. In contrast Ba_2IrO_4 [see Fig. 1(a)] is again free from distortions [8] and thus serves as a canonical system with a single Ir ion in the paramagnetic (PM) unit cell [9,10]. The AFM insulating phase of Ba_2IrO_4 has an Ir local magnetic moment of $0.34\mu_B$, with an easy axis perpendicular to the c axis [11], and is stable up to $T_N = 240$ K. Only a small charge gap of about $\sim$0.2 eV is deduced from angle-resolved photoemission spectroscopy (ARPES) measurements [9].

Theoretical studies of $(Ba,Sr)_2IrO_4$ based on variational Monte Carlo [12] as well as density functional theory (DFT) combined with dynamical mean-field theory [4,5,13] support the original heuristic picture of a correlation-mediated spin-orbit driven insulator. Therein the SOC discriminates the Ir $5d(t_{2g})$ into effective $J_{\text{eff}} = 1/2,3/2$ states [14]. While four electrons of Ir^{4+} fill up $J_{\text{eff}} = 3/2$ completely, one electron remains in $J_{\text{eff}} = 1/2$ at low energy. The interacting half-filled band at the Fermi level is then either gapped mainly due to the Slater mechanism forming an AFM state or directly by electronic correlations with secondary magnetic ordering.

Doping of the iridates is achievable [15], and recent experimental works succeeded to reveal a subtle electronic structure for both electron and hole doping [16–21]. By surface electron doping of Sr_2IrO_4 [16], the quasiparticle (QP) strength seems to vary along the Fermi surface, somehow reminiscent of the famous Fermi arcs known from hole-doped cuprates. Though effective hole-doping of Sr_2IrO_4 also shows k-selective features [17], the fermiology appears much more incoherent.

In this work we focus on single-layer tetragonal Ba_2IrO_4 as a test case for basic accounts on the intriguing spin-orbit assisted correlation physics. From the realistic band structure at stoichiometry, effective low-energy three- and one-band Hubbard models are constructed to assess the possible correlation regimes. Local and nonlocal self-energy representations are employed to study metal-insulator transition and doping effects. Fermi-surface differentiations in qualitative agreement with recent experimental findings are revealed. An obvious dichotomy in the doped fermiology between electron and hole doping is found at strong coupling, identifying the electron-doped case as the candidate for a proper analog to the hole-doped cuprates.

II. THEORETICAL FRAMEWORK

First-principles DFT calculations in the local density approximation (LDA) are performed for Ba_2IrO_4 in the $I4/mmm$ space group according to crystal data by Okabe *et al.* [8]. Computations are performed using a mixed-basis pseudopotential scheme [22,23] with [24] and without the inclusion of spin-orbit coupling. We construct maximally localized Wannier functions (MLWFs) [25] for the Ir $5d(t_{2g})$-based low-energy bands close to the Fermi level from LDA calculations without SOC. Therefrom an initial three-band Hubbard Hamiltonian in the original $5d(t_{2g})$ basis of orbitals $m,m' = yz,xz,xy$ and with local spin-orbit term on Ir sites i is drawn, i.e.,

$$H = \sum_{\mathbf{k}mm'\sigma} \varepsilon^{t_{2g}}_{\mathbf{k}mm'} c^{\dagger}_{\mathbf{k}m\sigma} c_{\mathbf{k}m'\sigma} + \sum_i \left(H^{(i)}_{\text{CF}} + H^{(i)}_{\text{SO}} + H^{(i)}_{\text{INT}} \right), \tag{1}$$

where $c^{\dagger}$, c are creation, annihilation operators for the MLWF states with spin projection $\sigma = \uparrow,\downarrow$. The t_{2g} dispersion $\varepsilon^{t_{2g}}_{\mathbf{k}}$ excludes on-site parts, which enter the crystal-field term H_{CF}. A Slater-Kanamori parametrization with Hubbard $U^{t_{2g}}$ and Hund's exchange $J^{t_{2g}}_{\text{H}} = 0.14$ eV [14,26] is used for H_{INT}, including density-density as well as spin-flip and pair-hopping terms. The SO interaction reads $H_{\text{SO}} = \lambda \sum_\nu \mathbf{s}_\mu \cdot \mathbf{l}_\mu$, where λ is the coupling constant and $\mathbf{s}$,$\mathbf{l}$ are spin-, angular-momentum operators. Because of the shift of $5d(e_g)$ to higher energies, restricting the general spin-orbit interaction matrix to the $5d(t_{2g})$ manifold is justified [12,27].

The full problem (1) is solved by mean-field rotational-invariant slave-boson (RISB) theory [28–30], using a

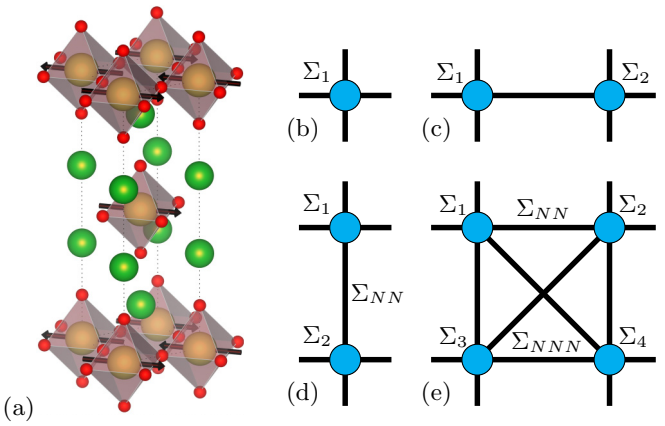

FIG. 1. (Color online) (a) Crystal and AFM structure of tetragonal Ba_2IrO_4, with Ba (green), Ir (brown), and O (small red) ions. (b)–(e) Utilized self-energy representations within the square lattice of an IrO_2 layer. (b) Single on-site and (c) two on-site self-energies, neglecting intersite terms. (d) NN two-site cluster and (e) four-site (2×2) self-energy.

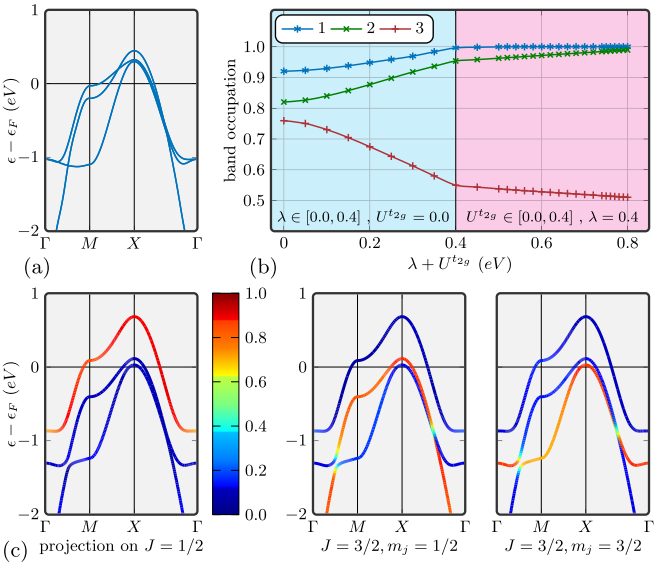

FIG. 2. (Color online) Dispersion and occupations within the iridate t_{2g} three-band manifold. (a) Bands without SOC; (b) band fillings with increasing SOC strength λ and Hubbard U (with "3" denoting highest band). (c) Effective-J weight on the respective bands.

multiorbital single-site self-energy [see Fig. 1(b)] for the correlated subspace of three effective t_{2g} orbitals. The method amounts to a distinction of the electron's QP (fermionic $f_{\nu\sigma}$) and high-energy excitations (taken care of by the set of local slave bosons $\{\phi\}$) on the operator level through $\underline{c}_{\nu\sigma} = \hat{R}[\{\phi\}]^{\sigma\sigma'}_{\nu\nu'} f_{\nu'\sigma'}$, where ν is a generic orbital/site index [30]. Self-energies with a term linear in frequency and a static part result in mean field. The RISB approach is especially suited to model anisotropic interactions [31], and here allows one to treat the interacting spin-orbit problem in complete generality, i.e., without abandoning off-diagonal terms. Neglecting H_{INT} leads to spin-orbit QP bands in very good agreement with the LDA+SOC low-energy dispersion.

For larger λ, the three-band Hamiltonian may be reduced to a tailored one-band problem for the effective $J = 1/2$ state at low energy. In this restricted orbital space we also allow for an enlarged correlated subspace in real space via clusters of two and four sites [see Figs. 1(d) and 1(e)]. Therewith nonlocal correlations up to next-nearest neigbor (NNN) are incorporated. The initial cluster embedding is of cellular type; k-dependent self-energies are obtained for the two-site ($\Sigma^{(2)}$) cluster and the four-site ($\Sigma^{(4)}$) cluster via further periodization using [32]

$$\Sigma^{(2)}(\mathbf{k},\omega) = \Sigma^{(2)}_{11}(\omega) + \Sigma^{(2)}_{12}(\omega)(\cos k_x + \cos k_y), \quad (2)$$

$$\Sigma^{(4)}(\mathbf{k},\omega) = \Sigma^{(4)}_{11}(\omega) + \Sigma^{(4)}_{12}(\omega)(\cos k_x + \cos k_y) + \Sigma^{(4)}_{13}(\omega)\cos k_x \cos k_y. \quad (3)$$

Since single-site RISB is equivalent to single-site DMFT with a simplified impurity solver, the cluster extension corresponds to cluster DMFT with the named restrictions in the self-energy representation. Albeit approximative, the cluster-RISB method has been proven capable to shed light onto relevant features of nonlocal correlation physics [30,33–35].

III. FROM THREE-BAND TO EFFECTIVE ONE-BAND PHYSICS

The LDA calculations for Ba_2IrO_4 reveal dominant t_{2g}-like bands at low energy, and a minor e_g-like electron pocket around Γ. Static DFT+U computations lead to an upward energy shift of the latter pocket into the unoccupied region. Thus that e_g-derived contribution plays no vital role in the key correlation physics and is neglected in the following. Figure 2(a) displays the MLWF-based t_{2g}-like low-energy bands adapted from LDA without SOC. Including spin-orbit coupling in the subsequent RISB treatment shifts the lower band manifold with effective $J = 3/2$ down in energy [see Fig. 2(b)]. Inclusion of H_{INT} shifts those bands even further away from the Fermi level ϵ_{F}, eventually resulting in completely filled $J = 3/2$ and half-filled $J = 1/2$ states [cf. Fig. 2(c)]. This limit may be understood from a constructive interplay between Hund's third rule and the minimization of Coulomb interactions in the Ir($5d^5$) shell. The orbital character of the remaining half-filled band at ϵ_{F} is indeed nearly exclusively of $J = 1/2$ kind. Due to its isolation, the low-energy physics of single-layer iridate can be further analyzed to a good approximation within a one-band picture. From the three-band calculation with $\lambda = 0.4$ eV and neglecting H_{INT}, we therefore Fourier transform the isolated $J = 1/2$ band to obtain a single-band tight-binding parametrization. In addition to a local Coulomb interaction scaling with a Hubbard U, a nearest-neighbor (NN) spin-spin interaction term is introduced to take care of the spin-orbit induced in-plane $J = 1/2$ pseudospin ordering [3]. The low-energy one-band iridate Hamiltonian is then given by

$$H_{1\mathrm{B}} = \sum_{ij\sigma} t_{ij} c^{\dagger}_{i\sigma} c_{j\sigma} + U \sum_i n_{i\uparrow} n_{i\downarrow} + \Gamma \sum_{\langle ij \rangle} S^{\parallel}_i S^{\parallel}_j, \quad (4)$$

where t_{ij} marks the hoppings of the underlying $J = 1/2$ dispersion with bandwidth $W = 1.55$ eV and $\Gamma > 0$ as the anisotropic AFM pseudospin coupling between the in-plane component $S^{||}$ of the pseudospins. The first near-neighbor in-plane hoppings amount to $(t,t',t'',t''') = (-205,-16,35,13)$ meV, and the interlayer coupling is given by $t_\perp = -11$ meV. Based on the work of Katukuri *et al.* [26], a value $\Gamma = 12$ meV is computed for the anisotropic interaction. Note that the effective one-band description does not allow one to discriminate between different ordering axes of the pseudospins; the definite in-plane easy axis remains arbitrary [26].

Albeit in the following we focus on in-plane aspects, the complete three-dimensional dispersion is included for deriving the effective one-band physics within mean-field RISB. Half filling is generally marked by the effective one-orbital occupation $n = 1$.

IV. EFFECTIVE ONE-BAND PHYSICS FROM SINGLE-SITE RISB

Let us first focus on the pure on-site self-energy treatments, neglecting intersite terms. Disregarding the spin-spin interaction, the PM Mott transition with vanishing QP weight $Z = [1 - \frac{\partial}{\partial\omega}\Sigma\,]^{-1}_{\omega=0}$ occurs at $U_{c,PM} = 2.85$ eV, i.e., $U_{c,PM}/W \sim 1.84$. To account for AFM order we use a $\sqrt{2}\times\sqrt{2}$ unit-cell architecture, treating two NN Ir ions with their respective on-site Σ [cf. Fig. 1(c)]. The anisotropic interaction between the pseudospins is chosen favorably along the x direction and handled in mean-field decoupling, i.e., $S_i^{(x)}S_j^{(x)} \to S_i^{(x)}\langle S_j^{(x)}\rangle$. At stoichiometry antiferromagnetism with staggered moments aligned along the x-axis marks the ground state for any $U > 0$. For $U_{c,AFM} = 0.8$ eV the system becomes insulating at a first-order transition [see Fig. 3(a)]. Thus the critical U for the metal-insulator transition (MIT) is strongly lowered when allowing for magnetic order. Figure 3(b) shows that the spin moment pointing along x becomes highly susceptible to small interaction changes around $U_{c,AFM}$, but saturates only at much larger interaction strength. Therefore, in this case the MIT is not of strong Mott type, i.e., does not result in complete electron localization. It has magnetic-driven signature, where the charge-gap opening results in the formation of increased-dispersive Slater-like bands [12]. Away from stoichiometry, the AFM order remains stable up to rather large doping, as long as $\langle S^{(x)}\rangle$ is finite. Symmetric 30% electron/hole doping is necessary to render $\langle S^{(x)}\rangle \to 0$ for $U = 1$ eV.

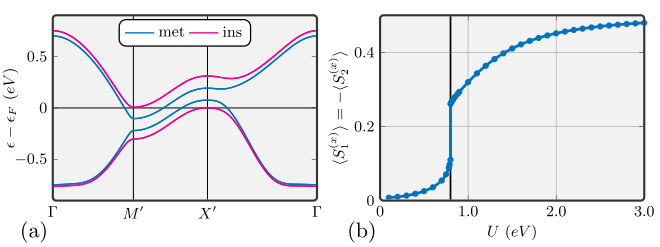

FIG. 3. (Color online) Two-single-site MIT with AFM order in the effective one-band model. (a) Metallic and insulating QP band structure for $U = 0.8$ eV. (b) Jump of $\langle S^{(x)}\rangle$ at the first-order MIT.

V. EFFECTIVE ONE-BAND PHYSICS FROM CLUSTER RISB

To evaluate the relevance of intersite self-energy contributions especially in the doped regime, we extend the one-band investigations towards computations within a cluster framework. Therein the pseudospin interaction term in Eq. (4) may be treated in complete many-body form on the local clusters. It is directed along x for the case of a two-site cluster, and symmetrically along x, y in the four-site cluster approach.

In the following the analysis of the self-consistent statistical weight of cluster multiplets via the resulting slave-boson amplitudes $\{\phi\}$ will prove useful. Note that the local cluster eigenstates can be written as $|\underline{\Gamma}\rangle \sim \sum_{\Gamma'}\phi_{\Gamma\Gamma'}|\mathrm{vac}\rangle|\Gamma'\rangle$, whereby Γ,Γ' share the same quantum numbers [30,34]. Here the eigenbasis is labeled by the set $\mathcal{B} = \{N,S^2,S_z,(H_{loc})\}$, with N as the total particle number, S^2 the total spin momentum, S_z its z component, and H_{loc} as the local energy. If in the following H_{loc} breaks spin symmetry, the resulting states are treated in a first-order perturbation approach.

There are 16 eigenstates on the two-site cluster and 256 on the four-site cluster. The statistical weight of states Γ_q with identical quantum numbers according to $\mathcal{B}$ is collected in the probability

$$\rho_q = \sum_{q'}\rho_{qq'}\delta_{qq'} = \sum_{q'p}\phi^*_{pq}\phi_{pq'}\delta_{qq'}, \tag{5}$$

with the normalization $\sum_p \rho_p = \mathrm{Tr}\,(\phi^\dagger\phi) = 1$.

A. Two-site cluster

Already the minimal in-plane two-site cluster involving NN Ir sites [cf. Fig. 1(d)] allows for insights on the key effects of an intersite self-energy Σ_{12}. At half filling, the PM Mott transition occurs at $U^{(2)}_{c,PM} = 1.5$ eV, accompanied by a jump of the already negative NN spin-correlation $\langle S_1S_2\rangle$ towards even lower values [cf. Fig. 4(a)]. This marks the dominance of the intersite singlet cluster state in the Mott-insulating regime (see below). When allowing for the AFM phase, Fig. 4(a) displays that the MIT occurs as in the two-single-site study at $U^{(2)}_{c,AFM} = U_{c,AFM} = 0.8$ eV.

In the doped cases, we focus on cluster effects in the PM phase. Figures 4(b) and 4(c) show key information on the significance of nonlocal self-energy terms for electron and hole doping. The on-site QP weight is lower in the electron-doped case for the same value of $U = 2.5$ eV, marking somewhat stronger electron correlations. Intersite (NN) QP weights become relevant for $U > 1$ eV. Their magnitude is sizable at small doping and negligible about 20% away from half filling. Note the sign change of Z_{NN} when going from hole to electron doping. For sizable U the two-particle singlet on the two-site cluster dominates the multiplet states at half filling ($n = 1$). With doping, increasing weight is transferred to the triplet as well as one(three)-particle states when adding holes(electrons). Also here there is a small electron-hole asymmetry: the singlet(triplet) is more(less) pronounced with hole than electron doping. Figure 5 shows for illustration the two-site cluster spectrum of relevant multipltes with the interacting Fermi level ε_F for 5% electron and hole doping, respectively. The multiplets form roughly two groups in

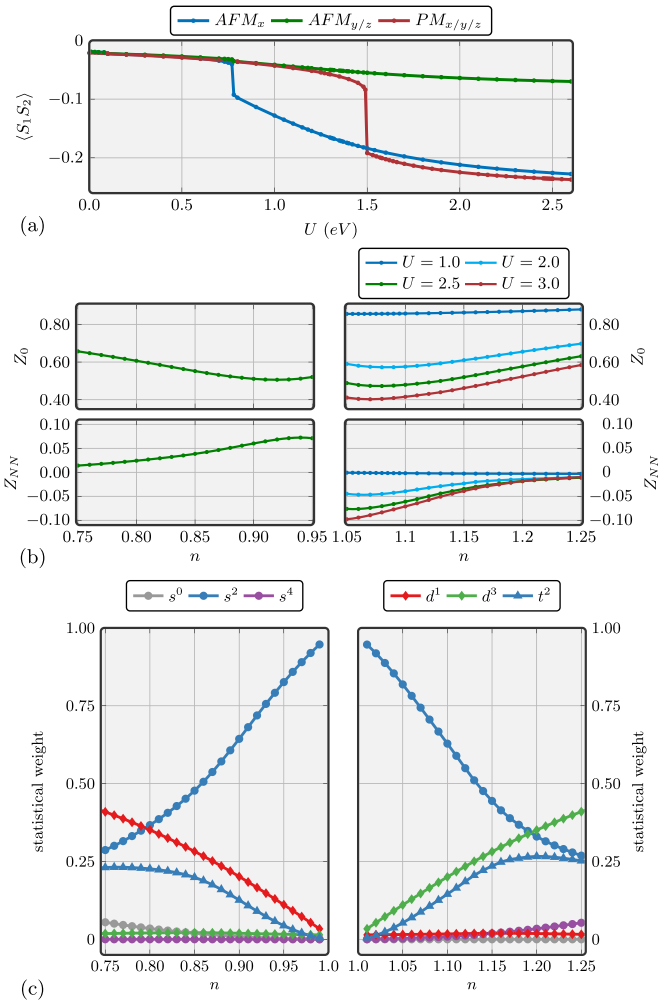

FIG. 4. (Color online) Two-site-cluster observables. (a) NN spin-correlation function at half filling. (b) Intra- and intersite QP weight for hole (left) and electron (right) doping from 5%–25%. The NN QP weights are positive (negative) for hole (electron) doping. (c) Statistics of cluster multiplets with hole (left) and electron (right) doping for $U = 2.5$ eV. Circles denote (s)inglet states, diamonds (d)oublets, and triangles (t)riplets. The particle sectors are color encoded and marked by the superscript numbers.

energy, split by the interaction $U = 2.5$ eV, understood from the involvment of doubly occupied sites in the higher energy group of states [34]. In the electron-doped case the multiplets are closer to ε_F in energy, reminiscent of the simple picturing of doping into the upper Hubbard band.

B. Four-site cluster

The four-site cluster is the proper minimal motive on the correlated square lattice and it is adequate to account for $d_{x^2-y^2}$-ordering tendencies in hole-doped cuprates [36]. We utilize it here to include NNN self-energy effects for doped iridates in the PM phase. The paramagnetic Mott transition at half filling is located at $U^{(4)}_{c,PM} = 1.95$ eV, correcting for the too dominant NN singlet formation in the two-site cluster approach.

In the four-site cluster description the correlation strength for the same value of U is generally enhanced compared to the

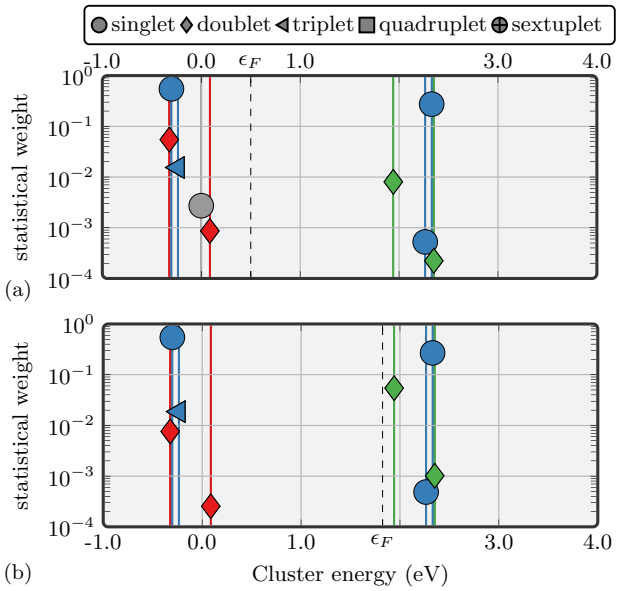

FIG. 5. (Color online) Two-site cluster spectra for $U = 2.5$ eV with filling (a) $n = 0.95$ and (b) $n = 1.05$, which amounts to 5% hole/electron doping. Colors and symbols mark states as described in Fig. 4(c).

two-site cluster approach, documented by the smaller on-site QP weight in Fig. 6(a). Moreover, the relation $|Z_{NNN}| > |Z_{NN}|$ holds for small doping, pointing towards anisotropic electron correlations in this regime. A larger correlation anisotropy is expected in the electron-doped compound because of the sign difference between Z_{NNN} and Z_{NN}. For any given symmetric doping the on-site Z is marginally lower for electron doping. The pseudospin anisotropy renders the calculations numerically more challenging and is thus only included at 5% doping. There it leads again to a marginal increase of correlation strength. The pseudospin correlation function $\langle S_i S_j \rangle$ on the four-site cluster depicted in Fig. 6(b) has strong AFM signature in NN distance and conclusively strong FM signature in NNN distance, both monotonically decreasing from half filling. With symmetric doping the respective pseudospin correlations are somewhat stronger in the electron-doped case. As expected, including the anisotropy term in the Hamiltonian strengthens the in-plane correlations, especially alongside the commensurate directions, i.e., along x for $\langle S_1 S_2 \rangle$ and along y for $\langle S_1 S_3 \rangle$. Though energetically no in-plane easy axis is favored, AFM order is numerically most easily stabilized with the experimental [110] easy axis.

Figure 6(c) shows the statistical weight of the four-site cluster multiplets with doping when neglecting the pseudospin anisotropy term. Dominant singlet states, now in the four-particle sector, rule again at small doping, but in contrast to the two-site cluster approach the triplet states take over beyond 5% hole or electron doping. Furthermore, including the NNN self-energy, connected to the NNN hopping, now leads to marginally stronger(weaker) triplets(singlets) in the hole-doped regime. Thus short-range spin flucuations should be slightly larger for hole doping. Charge fluctuations on the electron-doped side from the four-particle into the five-particle cluster sector are more pronounced than the symmetric

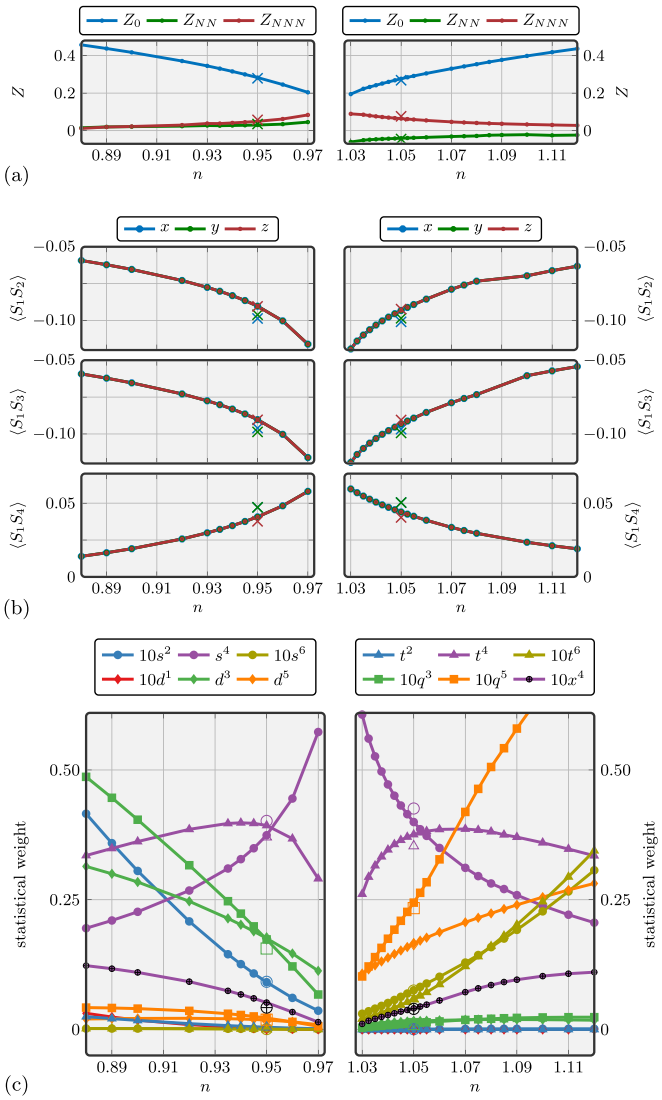

FIG. 6. (Color online) Four-site cluster observables for $U = 2.5$ eV. Left panels show hole doping; right ones electron doping. (a) QP weights without (full lines) and with inclusion of the pseudospin anisotropy term (large crosses). (b) NN and NNN pseudospin correlation functions $\langle S_i S_j \rangle$. (c) Statistics of cluster multiplets with hole (left) and electron (right) doping. The prefactor 10 denotes statistical weight multiplied by 10 for better visibility. Circles denote (s)inglets, diamonds (d)oublets, triangles (t)riplets, squares (q)uartets, and crossed circles sextuplets (x). Open symbols at 5% doping represent the matching states from inclusion of the pseudospin anisotropy.

fluctuations on the hole-doped side from the four-particle into the three-particle sector. Moreover, even fluctuations into the six-particle sector are taking place both into singlet and triplet states. With hole doping, only the two-particle singlet has some weight while the two-particle triplet is negligible. Eventual inclusion of the pseudospin anisotropy term enhances the singlet-triplet splitting in the dominant four-particle sector. At 5% doping, the interacting Fermi level is again located in higher energy block of multiplets for electron doping, while for hole doping it remains more or less in between both blocks of multiplets (see Fig. 7). Thus also in this larger-cluster

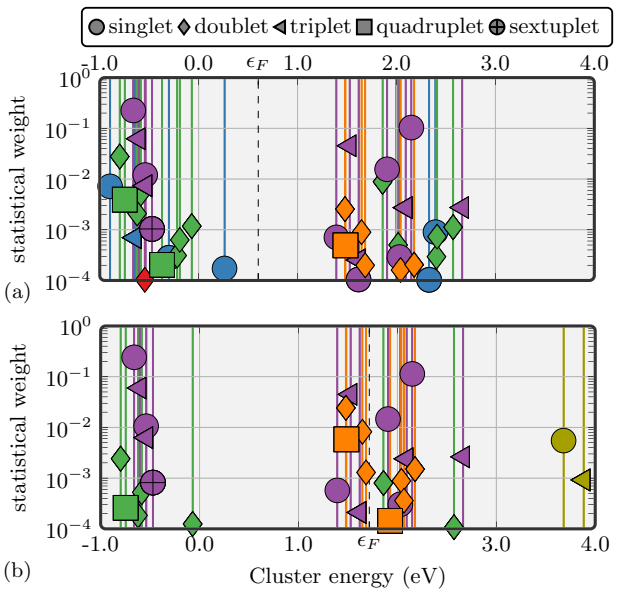

FIG. 7. (Color online) Four-site cluster spectra without pseudospin anisotropy for $U = 2.5$ eV. (a) $n = 0.95$ and (b) $n = 1.05$, which amounts to 5% doping, respectively. Colors and symbols mark states as described in Fig. 6(c).

approach a doped-Mott-insulator picture applies more to the electron-doped regime.

In order to assess the electronic correlation strength with hole and electron doping, still a further viewpoint can be taken. As discussed in previous works [37,38], the computation of the local von Neumann entropy S may provide a measure of correlation. The off-diagonal cluster density matrix $\rho_{qq'}$ [see Eq. (5)] may be used to compute S and relative entropies. After diagonalizing $\rho_{qq'}$, its eigenvalues ρ_λ are utilized to write the local von Neumann entropy via $S = -\sum_\lambda \rho_\lambda \ln \rho_\lambda$ as well as the relative entropy $\Delta S(\rho^A || \rho^B) = \sum_\lambda \rho_\lambda^A (\ln \rho_\lambda^A - \ln \rho_\lambda^B)$ for two systems A and B. The larger the relative entropy, the more distinct the two compared systems are.

Figure 8 shows that at low symmetric doping the entropy S is slightly smaller in the electron-doped case, rendering it more correlated. Inclusion of the pseudospin anisotropy again enhances the correlation effect. Albeit the electron-hole correlation asymmetry from entropy is small in absolute numbers, the relative entropy by comparison to the noninteracting case marks the electron-doped regime rather clearly as the one with increased correlation strength (see Table I).

Finally we want to discuss k-dependent signatures at finite doping based on the four-site cluster approach. In principle

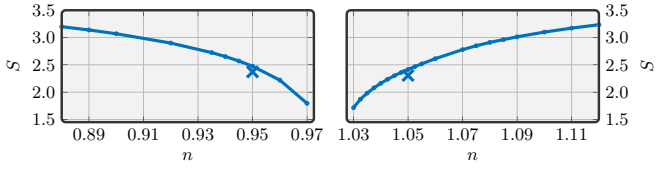

FIG. 8. (Color online) Local von Neumann entropy on the four-site cluster with doping. Crosses: with inclusion of the pseudospin anisotropy.

TABLE I. Local von-Neumann entropy at 5% symmetric doping including pseudospin anisotropy. The distribution ρ marks the interacting ensemble and ρ^0 is associated with the noninteracting ensemble of states.

Doping	$S(\rho)$	$S(\rho^0)$	$S(\rho\|\|\rho^0)$	$S(\rho^0\|\|\rho)$
−5%	2.37	4.04	1.63	0.0
+5%	2.31	4.08	2.18	0.0

two scenarios may hold: either doping right within the Slater-Hubbard bands takes place ($U \sim W$), or it results in the buildup of a renormalized FS readily from the original itinerant dispersion ($U \gg W$). In the first case, k-space differentiation occurs because of the energy dependence of the gap-forming bands [compare Fig. 3(b)]. Then here, hole(electron) doping would lead to FS pocket formation around $X'(M')$, as indeed verified by plotting the doped FS within our two-single-site approach in Figs. 9(a) and 9(b). Such a scenario apparently has been detected in ARPES measurements for effective *hole doping* of Sr_2IrO_4 [17].

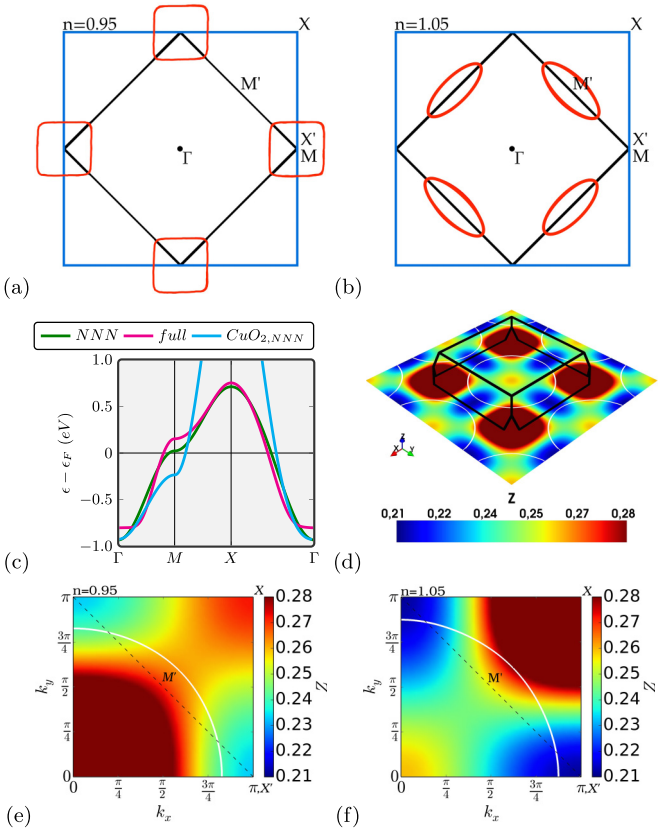

FIG. 9. (Color online) Iridate k selectivity. (a),(b) FS pockets from the two-single-site treatment for hole and electron doping at $U = 1$ eV. (c) NNN- and full-hoppings one-band dispersion compared with standard cuprate dispersion (CuO_2: $t = -430$ meV; $t' = +129$ meV [39]). (d) In-plane QP weight $Z(\mathbf{k})$ for $U = 2.5$ eV and electron doping $n = 1.05$; black line: Brillouin zone; white line: interacting FS. (e),(f) Magnified comparison in symmetry-inequivalent k-space sector, between (e) hole doping and (f) electron doping, both for $U = 2.5$ eV.

In the strong-coupling scenario, k selectivity in a one-band picture is usually due to finite intersite terms $\Sigma_{\alpha\beta} \neq 0$ for $\alpha \neq \beta$. We may encounter such effects via our periodized in-plane cluster self-energies. For instance, the QP weight $Z = Z(\mathbf{k})$ for the model (4) can vary based on NN and NNN self-energies of the four-site cluster. Figures 9(d)–9(f) display the obtained QP variations in the Brillouin zone without pseudospin anisotropy. As discussed before, inclusion of the latter generally leads to a minor increase of the overall correlation strength. Let's focus on the interacting fermiology, i.e., $Z = Z(\mathbf{k}_F)$, where $\mathbf{k}_F$ is the Fermi wave vector. For both dopings, i.e., hole- and electronlike, Figs. 9(e) and 9(f) show an obvious in-plane nodal/antinodal dichotomy. The QP weight on the FS along the node $(0,0) - (\pi/2,\pi/2)$ is larger than along the antinode $(0,0) - (0,\pi)$. Though the absolute differences are small within cluster RISB, it serves as a proof of principles for k-space differentiation by electronic correlations, in agreement with recent ARPES experiments on surface *electron-doped* Sr_2IrO_4 [16].

Second, there is a substantial quantitative difference in the k-space differentiation of $Z(\mathbf{k}_F)$ between both doping directions. The electron-doped case exhibits stronger QP-weight variation along ϵ_F than the hole-doped case. In other words, for same interaction strength, theory predicts that electron doping of single-layer iridates is more likely to cause a Fermi-arc structure than hole doping. This finding is reminiscent of the electron-hole dichotomy in cuprates [40,41], yet with a twist: in cuprates, the hole-doped case is assumed more susceptible to k-selective correlations. Generally, for all encountered symmetric doping distances from $n = 1$, the intrasite Z is always somewhat lower on the electron-doped side.

As pointed out before [7,12], the qualitative difference may be explained by the relevance of hopping characteristics beyond NN [42]. Because of the different sign of the NNN t' in both compound families, the enhanced correlation-susceptible van Hove singularity at M in reciprocal space is above(below) the Fermi level for iridates(cuprates) as shown in Fig. 9(c). Thus from a phase-space argument, hitting stronger correlations at the antinode takes place by electron(hole) doping of iridates(cuprates). The hoppings beyond NNN are then effective in shifting the iridate van Hove singularity further away from ϵ_F. Note that a recent extended fluctuation-exchange-based study [43] also found electron-hole doping asymmetries in Sr_2IrO_4.

VI. SUMMARY

An effective $J = 1/2$ low-energy one-band modeling is derived for single-layer iridates from the initial spin-orbit interacting t_{2g} manifold. For $U \lesssim 1.25$ eV Slater-like behavior dominates, while for $U \gtrsim 1.25$ eV Mott-Hubbard physics is more in control. In reality a subtle interplay between both limits is expected [6]. Our theoretical study reveals an electron-hole doping asymmetry approached from two directions. First the analysis of QP weights and local cluster states at strong coupling points to increased electronic correlations on the electron-doped side. Second, investigating the low-energy k-space differentiation also exposes a doping asymmetry, taking place at weaker as well as at stronger coupling and has partly already been confirmed by recent experiments [16,17].

Fermi-surface pockets that occur for weaker electron-electron interaction are more likely for hole doping, whereas Fermi arcs may set in for stronger interaction with higher tendency again on the electron-doped side. Therefore, electron-doped iridates are candidates for a possible analog to hole-doped cuprates. The inclusion of the small pseudospin anisotropy is shown to somewhat increase the correlation strength, but no drastic qualitative changes arise therefrom at the present level of modeling.

ACKNOWLEDGMENTS

We are indebted to F. Baumberger, M. Behrmann, L. Boehnke, D. S. Dessau, R. Heid, and A. I. Lichtenstein for helpful discussions. This research was supported by the DFG-FOR1346 project. Computations were performed at the North-German Supercomputing Alliance (HLRN) under Grant No. hhp00031.

[1] M. K. Crawford, M. A. Subramanian, R. L. Harlow, J. A. Fernandez-Baca, Z. R. Wang, and D. C. Johnston, Phys. Rev. B **49**, 9198 (1994).
[2] B. J. Kim, H. Jin, S. J. Moon, J.-Y. Kim, B.-G. Park, C. S. Leem, J. Yu, T. W. Noh, C. Kim, S.-J. Oh, J.-H. Park, V. Durairaj, G. Cao, and E. Rotenberg, Phys. Rev. Lett. **101**, 076402 (2008).
[3] G. Jackeli and G. Khaliullin, Phys. Rev. Lett. **102**, 017205 (2009).
[4] C. Martins, M. Aichhorn, L. Vaugier, and S. Biermann, Phys. Rev. Lett. **107**, 266404 (2011).
[5] R. Arita, J. Kunes, A. V. Kozhevnikov, A. G. Eguiluz, and M. Imada, Phys. Rev. Lett. **108**, 086403 (2012).
[6] D. Hsieh, F. Mahmood, D. H. Torchinsky, G. Cao, and N. Gedik, Phys. Rev. B **86**, 035128 (2012).
[7] H. Watanabe, T. Shirakawa, and S. Yunoki, Phys. Rev. Lett. **110**, 027002 (2013).
[8] H. Okabe, M. Isobe, E. Takayama-Muromachi, A. Koda, S. Takeshita, M. Hiraishi, M. Miyazaki, R. Kadono, Y. Miyake, and J. Akimitsu, Phys. Rev. B **83**, 155118 (2011).
[9] S. Moser, L. Moreschini, A. Ebrahimi, B. D. Piazza, M. Isobe, H. Okabe, J. Akimitsu, V. V. Mazurenko, K. S. Kim, A. Bostwick, E. Rotenberg, J. Chang, H. M. Rønnow, and M. Grioni, New J. Phys. **16**, 013008 (2014).
[10] M. Uchida, Y. F. Nie, P. D. C. King, C. H. Kim, C. J. Fennie, D. G. Schlom, and K. M. Shen, Phys. Rev. B **90**, 075142 (2014).
[11] S. Boseggia, R. Springell, H. C. Walker, H. M. Rønnow, C. Rüegg, H. Okabe, M. Isobe, R. S. Perry, S. P. Collins, and D. F. McMorrow, Phys. Rev. Lett. **110**, 117207 (2013).
[12] H. Watanabe, T. Shirakawa, and S. Yunoki, Phys. Rev. Lett. **105**, 216410 (2010).
[13] H. Zhang, K. Haule, and D. Vanderbilt, Phys. Rev. Lett. **111**, 246402 (2013).
[14] N. B. Perkins, Y. Sizyuk, and P. Wölfle, Phys. Rev. B **89**, 035143 (2014).
[15] O. B. Korneta, T. Qi, S. Chikara, S. Parkin, L. E. DeLong, P. Schlottmann, and G. Cao, Phys. Rev. B **82**, 115117 (2010).
[16] Y. K. Kim, O. Krupin, J. D. Denlinger, A. Bostwick, E. Rotenberg, Q. Zhao, J. F. Mitchell, J. W. Allen, and B. J. Kim, Science **345**, 187 (2014).
[17] Y. Cao, Q. Wang, J. A. Waugh, T. J. Reber, H. Li, X. Zhou, S. Parham, N. C. Plumb, E. Rotenberg, A. Bostwick, J. D. Denlinger, T. Qi, M. A. Hermele, G. Cao, and D. S. Dessau, arXiv:1406.4978.
[18] J. He, H. Hafiz, T. R. Mion, T. Hogan, C. Dhital, X. Chen, Q. Lin, M. Hashimoto, D. H. Lu, Y. Zhang, R. S. Markiewicz, A. Bansil, S. D. Wilson, and R.-H. He, Sci. Rep. **5**, 8533 (2015).
[19] V. Brouet, J. Mansart, L. Perfetti, C. Piovera, I. Vobornik, P. L. Fèvre, F. Bertran, S. C. Riggs, M. C. Shapiro, P. Giraldo-Gallo, and I. R. Fisher, arXiv:1503.08120.
[20] A. de la Torre, S. M. Walker, F. Y. Bruno, S. Ricco, Z. Wang, I. G. Lezama, G. Scheerer, G. Giriat, D. Jaccard, C. Berthod, T. K. Kim, M. Hoesch, E. C. Hunter, R. S. Perry, A. Tamai, and F. Baumberger, arXiv:1506.00616.
[21] Y. K. Kim, N. H. Sung, J. D. Denlinger, and B. J. Kim, arXiv:1506.06639.
[22] S. G. Louie, K. M. Ho, and M. L. Cohen, Phys. Rev. B **19**, 1774 (1979).
[23] B. Meyer, C. Elsässer, F. Lechermann, and M. Fähnle, FORTRAN 90 Program for Mixed-Basis-Pseudopotential Calculations for Crystals, Max-Planck-Institut für Metallforschung, Stuttgart (unpublished).
[24] R. Heid, K.-P. Bohnen, I. Y. Skyladneva, and E. V. Chulkov, Phys. Rev. B **81**, 174527(R) (2010).
[25] N. Marzari, A. A. Mostofi, J. R. Yates, I. Souza, and D. Vanderbilt, Rev. Mod. Phys. **84**, 1419 (2012).
[26] V. M. Katukuri, V. Yushankhai, L. Siurakshina, J. van den Brink, L. Hozoi, and I. Rousochatzakis, Phys. Rev. X **4**, 021051 (2014).
[27] J.-M. Carter, V. Shankar V., and H.-Y. Kee, Phys. Rev. B **88**, 035111 (2013).
[28] T. Li, P. Wölfle, and P. J. Hirschfeld, Phys. Rev. B **40**, 6817 (1989).
[29] J. Bünemann, W. Weber, and F. Gebhard, Phys. Rev. B **57**, 6896 (1998).
[30] F. Lechermann, A. Georges, G. Kotliar, and O. Parcollet, Phys. Rev. B **76**, 155102 (2007).
[31] S. Schuwalow, C. Piefke, and F. Lechermann, Phys. Rev. B **85**, 205132 (2012).
[32] G. Biroli, O. Parcollet, and G. Kotliar, Phys. Rev. B **69**, 205108 (2004).
[33] F. Lechermann, Phys. Rev. Lett. **102**, 046403 (2009).
[34] M. Ferrero, P. S. Cornaglia, L. De Leo, O. Parcollet, G. Kotliar, and A. Georges, Phys. Rev. B **80**, 064501 (2009).
[35] I. I. Mazin, H. O. Jeschke, F. Lechermann, H. Lee, M. Fink, R. Thomale, and R. Valenti, Nat. Commun. **5**, 4261 (2014).
[36] A. I. Lichtenstein and M. I. Katsnelson, Phys. Rev. B **62**, R9283(R) (2000).
[37] K. Byczuk, J. Kunes, W. Hofstetter, and D. Vollhardt, Phys. Rev. Lett. **108**, 087004 (2012).
[38] P. Thunström, I. Di Marco, and O. Eriksson, Phys. Rev. Lett. **109**, 186401 (2012).
[39] E. Pavarini, I. Dasgupta, T. Saha-Dasgupta, O. Jepsen, and O. K. Andersen, Phys. Rev. Lett. **87**, 047003 (2001).
[40] N. P. Armitage, P. Fournier, and R. L. Greene, Rev. Mod. Phys. **82**, 2421 (2010).
[41] C. Weber, K. Haule, and G. Kotliar, Nat. Phys. **6**, 574 (2010).
[42] S. Pathak, V. B. Shenoy, M. Randeria, and N. Trivedi, Phys. Rev. Lett. **102**, 027002 (2009).
[43] H. Wang, S.-L. Yu, and J.-X. Li, Phys. Rev. B **91**, 165138 (2015).